Shape self-sensing with mutual inductance sensor array

M Soleimani [1], G Dingley[1], E Semaj[1], M Petrou[1]

Abstract—**Real-time sensing of shape is an important tool for many intelligent machines, particularly in soft robotics. Mutual induction data from an array of sensors shows great promise as an accurate tool for shape sensing. In this paper, we show how inductive array data can be used for shape imaging and topographic shape tracking. The idea has been extended to many geometrical settings showing a versatile tool for shape sensing. The sensors are arranged around a circular array allowing reconstruction of the deformation from circular shape to generic polygon shape including elliptic shape. A linear array shows the sensing of tension force and various deformation of lines. Finally, the sensor array is used on a surface allowing reconstruction of both shear force and the normal force to the surface. A suitable method of calculation of the mutual inductance between two coils has been implemented and a range of methods including inversion algorithms, calibration methods, and a machine learning tool show the application of the new shape sensor system.**

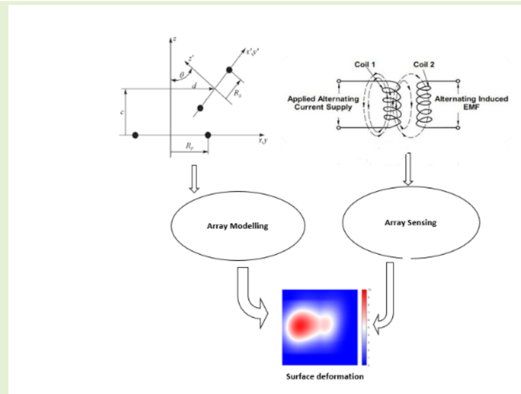

Index Terms— Magnetic induction array, shape tracking, linear and nonlinear inversion, soft robotics

I. Introduction

MAGNETIC induction sensors are used in a wide range of new industrial applications in the metal industry [1], [2]. There are several applications where shape tracking can play a critical role, which inspires the development of inductive shape sensing in this work. A versatile and multi-geometry shape-tracking tool is being developed in this work, demonstrating their possible use in various areas.

Balloon catheters are used in minimally invasive surgery to open and fix patency to the blocked lumen inside the body. During percutaneous transluminal angioplasty (PTA) an inflated balloon is used to remove the blockage caused by a stricture or plaque in the periphery or coronary vessels [3], [4], [5]. So the exterior shape of the balloon is an important factor. In [3] electrical impedance tomography sensor is proposed for such an application. Here we demonstrate the use of a magnetic inductive sensor array for such an application.

Robotic manipulators and arms have been very well adapted to factory environments. Most of these are rigid and can be tracked well with a vision system or based on dynamic motion modeling. Adaptation of soft robotics for doing similar tasks to humans and working with humans is the most recent trend in robotics with soft manipulators [6], and [7]. These applications are the main purpose for us to demonstrate the usage of a linear sensor array that can work in a wide of geometrical deformations. Demonstration of the capacitive measurement-based shape sensing was shown in [8], [9] and an impedance tomography-based sensor was shown in [10]. While the capacitive-based sensor has an inherent 3D sensing capability [10] it will be vulnerable to almost all types of surrounding materials, and an impedance tomography-based sensor will not have an inherent 3D sensing capability. However, the inductive array will be affected by only magnetic and metallic materials in its surroundings, but not affected by other materials such as plastics, liquids, and organic matter.

Tracking the touch and shape changes on a surface is of great interest in many application areas.

A planar shape and force sensing has many applications including the detection of skin damage for diabetes with sensors in their shoe sole [11]. A magnetic induction tomography with metallic interface skin was developed in [12] and touch force sensing was demonstrated in capacitive tomography in [9]. In this work, we show the self-sensing with the inductive array where the additional interfacing layer is not needed.

Focusing only on embedded shape sensors, for soft robotics, we can easily say that shape tracking is one of the essential sensing tasks. It is essential to ensure the deformability of the body of the sensor that goes with such deformability of the soft actuation bodies [13]. Shape sensing is required for the soft robots to detect their configuration, which is used for control of displacement and interaction with their environment. Shape

Paper submitted on xxxxx.

All authors are with the Electrical and Electronic Engineering Department, University of Bath, UK. (e-mail: m.soleimani@bath.ac.uk)

sensing systems existing in research literature primarily use a distribution of sensors to reconstruct the deformation, such as strain gauges [14], and accelerometers [15]. Either many sensors are used or the sparse nature of information from sensors limits the sensing methods. It is often challenging to have a high spatial sensing density. The imaging-inspired arrays allow optimization and automation of the sensing process without the requirement for a large number of sensors.

The article's main objective is to show the feasibility of using an inductive sensor array for shape sensing. A flexible sensor design as well as multiphysics modeling with deformation is the subject of future studies. The article is arranged in the following way. Section II describes the measurement system and the shape reconstruction process and provides insight into linear and nonlinear inversion algorithms. Section III shows the linear and nonlinear shape reconstruction algorithm used in this study. Section IV shows the experimental results, discussions are presented in section V, and the conclusions are drawn in Section VI.

II. Inductive Sensing System

Mutual inductance between coils is dependent upon their relative positioning to one other and also angular orientation. Therefore it is possible to derive spatial information from a measurement of mutual induction, either directly or by measurement of the induced voltage. Further, by arranging a number of coils into an array, a measurement of the mutual induction between the coils gives information relating to the deformation of the array shape. Applying the inverse processes to measurements taken with magnetic induction tomography (MIT)-style instrumentation [1], [2], the deformed array shape is therefore reconstructed.

A. The hardware system

The measurement system consists of (i) an array of equally spaced inductive coils arranged around the object periphery, (ii) a purpose build data acquisition system, and (iii) a host computer; as shown in Fig. 1a and the dimensions for each coil is given in Fig. 1b. Coil positions forming a circular deformable array, see photograph in Fig. 7, are shown in Fig. 1d, while Fig. 1c shows the linear array photographed in Fig. 14a. A surface membrane array shown in Fig. 8 has the coil positions indicated in Fig. 1e.

One of the eight inductive coils is supplied with an alternating current of 100 mA and the operational frequency is 55 kHz. For the eight channels MIT system, there are 28 unique coil pairs. 1-2, 1-3, …, 1-8, 2-3, 2-4, …, 7-8, giving 28 independent measurements. The image reconstruction module extracts 28 independent measurements to perform the reconstruction algorithm and displays and updates the images. Frame data is created by collecting N data points, where each point is a coil pair, consisting of one incident field coil and one detector coil, where $N=n(n-1)/2$ for n coils form the array.

The signal-to-noise ratio (SNR) between sensors is calculated to show the signal level of the system to the background noise level that is experienced. The SNR can be calculated using.

$$SNR_{dB} = \frac{1}{N}\sum_{i=1}^{N} 10\,log\left(\frac{\frac{1}{K}\sum_{j=1}^{K}(V_{i,j})}{\sqrt{\sum_{j=1}^{K}(V_{i,j})((V_{i,j}-\bar{V}_i)^2)}}\right) \quad (1)$$

Where N is the number of voltage measurements in one frame, K is the number of frames that a signal to noise ratio was calculated over and V is the collection of voltage measurements acquired during data collection. In addition to the effect of the external interferences, the SNR will also depend on the sensor arrangement and the geometry and number of sensors in given available space. The SNR for circular array (Fig. 1b) is between 50 dB (for measurement between two opposite coils) and 80 dB (for measurement between two neighboring coils) in a circular array setup. Fig. 1e shows the SNR values for 28 measurements from planar sensor Fig. 1d. This analysis can be done directly from measurement data and provide a good indicator of the data stability in each given sensor set up.

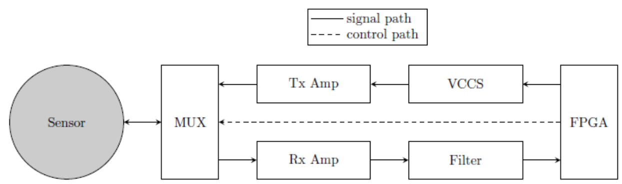

(a)

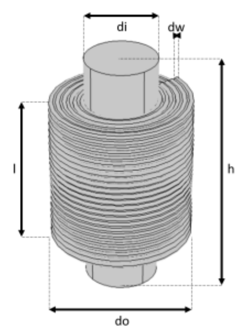

Parameter	Symbol	Value
Wire diameter	dw	32 AWG
Coil inner diameter	di	2.5 mm
Coil outer diameter	do	5 mm
Coil length	l	5 mm
Core height	h	8 mm
Case inner diameter	Dix	15 mm
Case outer diameter	Dox	40 mm
Case slot diameter	Dx	7 mm
Case height	Hx	10 mm
Number of turns	N	100

(b)

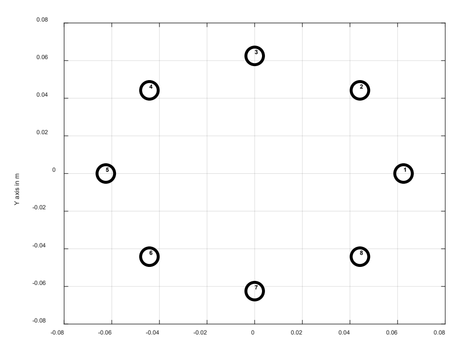

(c)

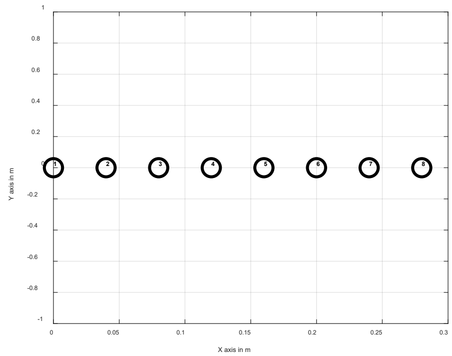

(d)

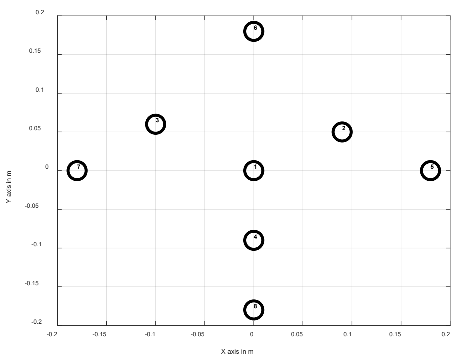

(e)

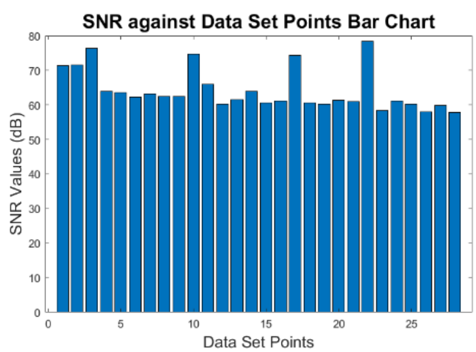

(f)

Fig. 1: (a)Measurement system architecture (b) sensor coil, (c) sensor initial position in ring array, (d) a linear array and (e) on a 2D surface array, (f) SNR for 2D surface array

B. The forward model

In [16] a suitable formula was demonstrated for the mutual inductance of pairs of coils. This stems from earlier work done by much earlier works [17], [18]. The actual numerical value for each point in the frame data is the magnitude of the voltage induced in the detector coil, v, by the current flowing in the incident field coil i and the mutual induction between the two M, given by:

$$\boldsymbol{v = i\omega M}. \tag{2}$$

Where ω is the angular frequency of the incident field, which along with i are constant during an array scan, therefore v is a function of coil-pair mutual inductance M. Mutual induction is dependent upon coil diameter, length, cartesian displacement, and relative angular orientation. Babic et al describe an analytic model for the mutual induction between circular current filaments, of radius R_p and R_s, with axial displacement d, The distance between the coils' centers is c, and relative angular orientation θ, given by [16]:

$$\boldsymbol{M = \frac{2\mu_0}{\pi}\sqrt{R_p R_s}\int_0^{\pi}\frac{\left[\cos(\theta)-\frac{d}{R_s}\cos(\phi)\right]\Psi(k)}{k\sqrt{V^3}}\,d\phi} \tag{3}$$

where $\Psi(k)$ is a function containing elliptic integrals, while k and V are functions of R_p, R_s, d, ϕ, and the distance between filament planes.

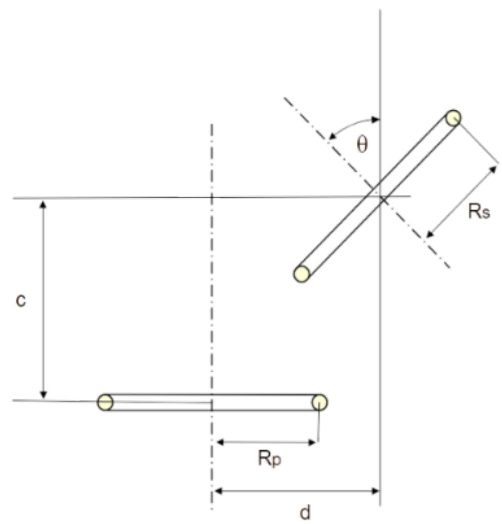

Fig. 2: Diagram indicating the parameters in describing the relative positioning and orientation of filament-loops

It is found that array coils can be approximated by two circular filaments, separated by a distance equal to the coil length, rather than representing each turn as an individual filament. With this approximation, only two filaments per coil are required in the model, such that the number of turns in the physical coil approximately represents only a scaling factor.

Fig. 3 shows the plot of measured frame data and simulated frame data from the mutual inductance analytic model with the two filament-loop approximation.

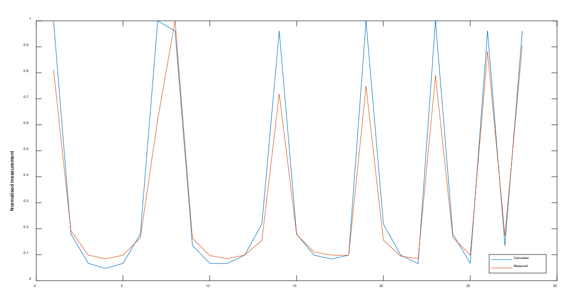

Fig. 3: Plot of calculated and measured frame data for the 8-channel circular sensor array from Fig1.b

III. Shape Reconstruction

Magetic inductive sensor system utilizes an array of inductive coils, distributed equally around an imaging region, to visualize the electromagnetic property distribution of the electrical conductivity of an imaging subject.

A. The inverse problem approach

The inverse problem in sensor array is defined as the retrieval of the unknown coil positions of the target from the measured voltage V_m:

$$\boldsymbol{V_m} - \boldsymbol{F}\,(\boldsymbol{x_0}) = \boldsymbol{J}(\,\boldsymbol{x} - \boldsymbol{x_0}) \qquad (4)$$

where x_0 is the initial estimated position, $F(x_0)$ is the initially estimated voltage obtained from a forward problem, and J is the Jacobian matrix obtained from a forward problem. Equation (2) links the mutual inductance between two coils to their geometrical positioning, depending on shape sensing geometry a Jacobian matrix J can be produced according to the possible shape change with perturbation. A standard Tikhonov regularisation method [2], [12] can then be used to estimate the geometrical changes ($\boldsymbol{x}$) for linear reconstruction in real-time. A nonlinear Gauss-Newton algorithm can also be used though it will take longer than expected for real-time devices to converge. In this case ($\boldsymbol{x}$) can be a geometrical representation of each pair of two coils based on diagram shown in Fig. 2. This way we can recover many shapes as long as the flexible domain stay connected to the coil array. In this paper we do not consider the mechanical properties of the soft domain, instead focusing on the geometrical displacement alone. However such mechanical modelling is important and will be addressed in future studies.

B. Calibration approach

A calibration test was completed in order to allow the sensors to detect their location. This test consisted of attaching two sensors to a set of callipers, then adjusting to a known distance; Fig. 4 shows a calibration process for a linear sensor.

(a)

(b)

Fig. 4: Image showing the maximum reading position of the sensors, (a) short distance between two coils, (b)longer distance between two coils. Actuation and measurement of sensor separation furnished by calipers.

Distances were measured from the center of the sensors, where the sensor diameter is 0.5cm, therefore if the calipers are set at a distance of 2cm, the distance between the two sensors would be 2.5cm. Setting the sensors at a known distance, the measured induced voltage was recorded; data was collected from 2cm to 10cm in 0.2cm intervals. Additionally, the test was repeated three times and for each reading, 10 values of induced voltage were measured for each distance, from which an average was taken. The collected data is shown in Fig. 5. Using a curve fitting algorithm, the function of the curve shown in Fig. 5 is given by:

$$\boldsymbol{y = 1663x^{-0.9646} + 1.575} \qquad (5)$$

Where y is the distance between two sensors and x is the recoded measured value in the MIT device representing the induced voltage measured between two sensors. In MIT device used in this study 2^{15}= 32768 represnts 5 V rms volatage. The calibration function with R^2=0.9923 wa fitted here.

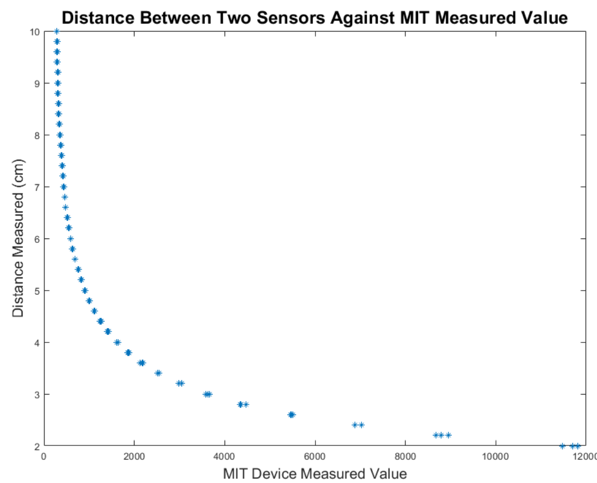

Fig. 5 Calibration plot for measured data from 16-digit ADC in digital form vs measured distance

This calibration test has allowed an accurate analysis of the sensors' original location. For example, Fig. 6a shows the expected location of the sensors when they are placed in a linear formation with 4 cm horizontal distance apart. This small difference can be a result of the manual sensor assembly, which has been identified by the calibration based inversion. While in Fig 6a we found the correct location of snesors from calibration function in Fig 6b the reconstrucrui of stretch is shown. In Fig 6c and Fig 6d we can reconstruct the bendig of the straight line

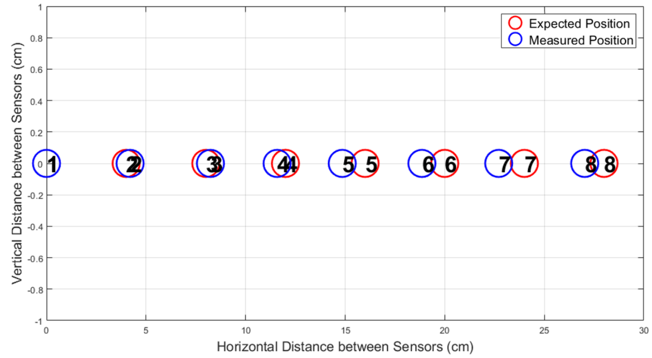

(a)

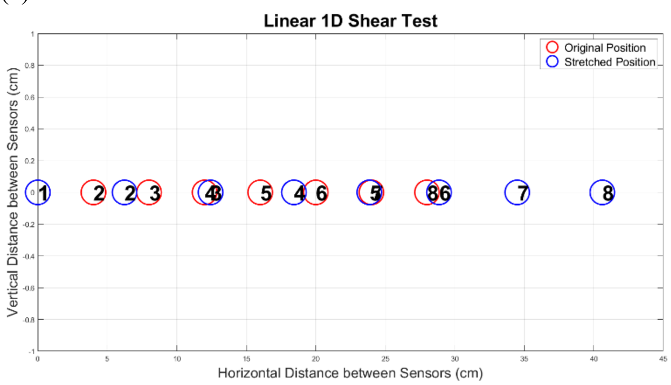

(b)

(c)

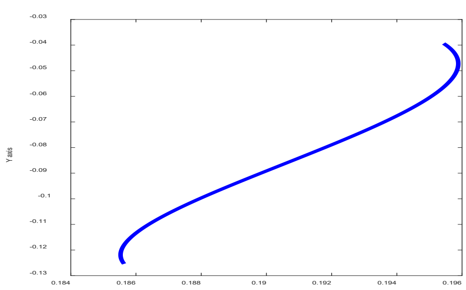

(d)

Fig. 6: (a) Plot of expected and simulated location of sensors for the sensors placed 4 cm apart. (b) tracking the stretched sensors, (c) bending from the straight line, (d) reconstruction of shape change from a straight line shown in part (c)

IV. SHAPE RESULTS

In this study, we deal with the geometrical orientation of two coils concerning their mutual inductance. A topological derivative function has been calculated based on the mutual inductance calculation allowing for both linear (real-time) and fully nonlinear reconstruction of the position of the coil sensors.

A. Ring array sensor

Inspired by a medical robotic application we focus on shape change from a circular array. Incorrectly shaped and sized balloon catheters can lead to unnecessary damage, yet even with preoperative imaging, the correct selection of size and shape of the balloon remains a challenge. A shape-sensing device could help with real-time feedback during surgery. Fig. 7 shows the reconstruction of the shape on a 2D circular ring array. Here we plotted some deformations from the initial circular shape, which is selected from real-time testing. In this case, the geometrical variables can be described in terms of x and y positions of 8 sensor coils. For an array set up around a circle with a diameter of 4.5 cm, a position accuracy of 1mm can be achieved for sensor's position displacement using a linear Thikhonov regularisation based inversion. In this case 5000 frames of shape data was collected and we show the frame 1000, 2000, 3000, each representing a variation from a circular shape

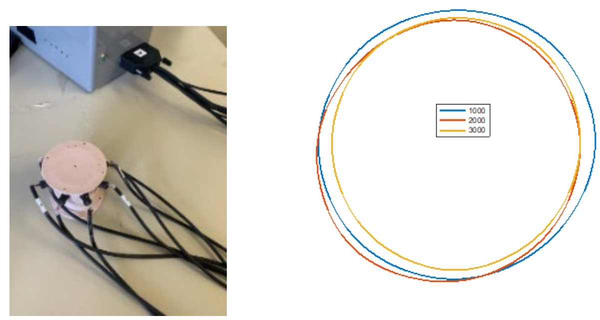

Fig. 7: Shape recording on a circular array

B. Sensors on a plane

Another key goal for this paper is to produce a surface that can detect when a normal force is applied. This is important as the normal force gives the user important information about the surface that can be used in multiple applications to produce useful information. The calculation for normal force occurs by measuring the vertical displacement of the surface on the z-axis. Fig 8. Shows the representation of the normal force of the touch in a single frame image. In Fig 9 we show the slice through 100 frames of image, while the image in fig. 9a represents a frequent touch to the sensor array. Fig. 9b includes a constantly increasing force and Fig. 9c represents an increase and decrease in the applied force.

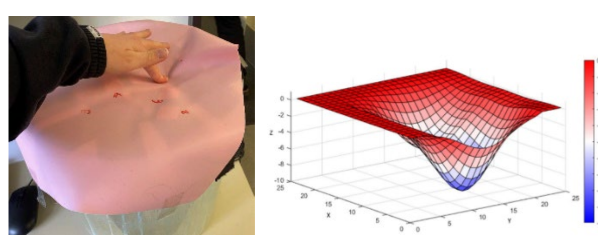

Fig. 8: Sensor position and normal force

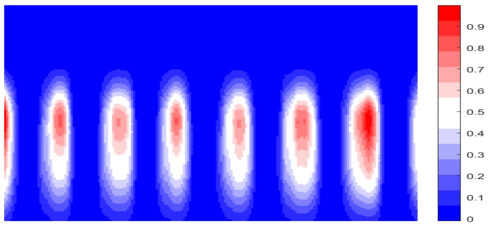

(a)

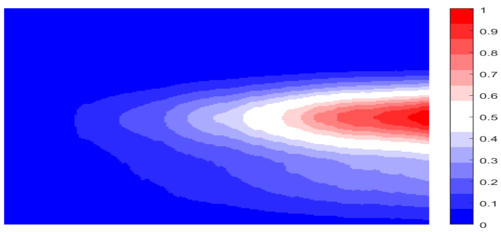

(b)

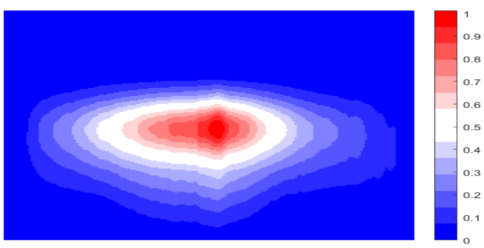

(c)

Fig 9: (a) Alternating force, (b) Increasing force, (c) increasing and then decreasing force.

In Fig. 10 we systematically increase the force, i.e. gravitational force as weight is added to the plane. As the force increases from 0 N to 7.2 N, the image scale is calibrated against the real applied force. We have repeated these experiments 40 times for each point of force to include error bars in the plot for calibration in Fig 10b. A linear calibration function with R^2=0.9969 and the function

$$\boldsymbol{y = 0.51x + 0.012} \qquad (6)$$

In this case x is the pixel value for the image (smoothed with neighboring pixels) and y is the predicted force in N.

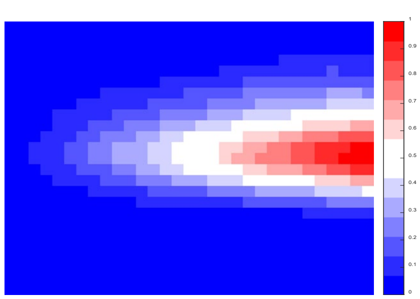

(a)

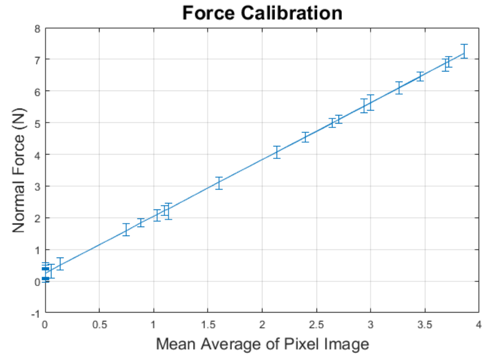

(b)

Fig 10. Calibration for force in the normal direction

Fig. 11 shows the detection of shear force, but in reality, only the displacement of the sensors using the calibration plot presented in Fig. 5 and the measured data are shown. Using the calibration system, the arrays were stretched in one direction to demonstrate the change in sensor location.

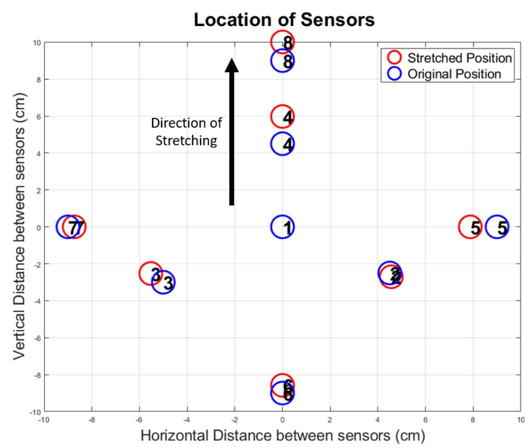

Fig 11. Displacement of the sensors due to a shear force applied in-plane of the sensor array

C. Sensor with actuation

Artificial muscles, much like natural muscles, are actuators that produce a change in their body shape, through expansion, contraction, or bending of the device. Artificial muscles can be actuated by various external stimuli, of which the most common are electrical, fluidic, and thermal stimuli. Pneumatic artificial muscles were used in the designed soft actuator. Pneumatic actuators are advantageous due to their high-power density, large force, high force-to-weight ratio, and desirable inherent compliance. They are relatively simple operation mechanisms, and much research has been done on this type of soft robotic mechanism. The most significant disadvantage of such devices is that bulky compressing systems and reservoirs are required to supply pressurized fluid, making portability limited and the system must be airtight to ensure there are no leakages to maximize output power. The soft actuator designed here is comprised of two pneumatic artificial muscles, made using Dragon Skin 20 silicone elastomer. The artificial muscles contain 6 chambers to maximize bending motion and an air chamber of 1.991mm, with an overall size of 15×35×70 mm, to increase the force with respect to pressure input. All molds were designed in Fusion 360 and actuators were built using silicone fabrication methods. Fig. 12 shows the mold used for the actuator design and Fig. 13 shows the soft actuator.

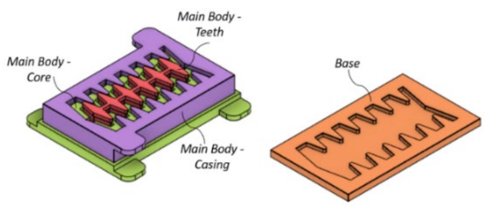

Fig. 12: Diagram detailing the different components that make up the mold for the final segment design.

Fig 13: The soft actuator, a two-channel pneumatic actuator made of Dragon Skin 20 Silicone Elastomer. Pneumatic tubing on either side with a diameter of 3mm and attached to the actuator using cable ties and silicone glue.

The sensor array system was secured to the soft actuator using string as shown in Figure 14(a). An Arduino UNO is used to control the actuation of the muscles, where relay modules are used to switch vacuum pumps on and off. All pumps are controlled by analog pins on the Arduino. The vacuum pumps operate at 12V and 12W, resulting in a current of 1A being pulled through the system when powered. To actuate a segment, 2 pumps were used in series resulting in a large current, 2A, being pulled through the system. To eliminate the current sink generated by actuating both muscles in the segment simultaneously a transistor was placed between the Arduino input pin and the vacuum pumps. For this experiment, the segment was actuated using the vacuum pumps powered to 8V, as higher voltages strain the actuator and risk tearing the silicone. The Arduino UNO controlled the activation of the pump such that the segment was actuated at a sequence of three different frequency stretches (0.25 Hz, 0.5 Hz, and 1 Hz) that were set for 36 seconds followed by a 4-second delay where the muscle remained un-actuated, which was successfully identified and measured by the sensor system as shown in Fig 14. Fig 14b shows the time domain displacements measured by the sensor which shows the changing frequency over the pre-set period. Fig 14c, d and e are the frequency domain representations of Fig 14b for each 36 second period, showing the peak of the frequency distribution at the appropriate values. The displacement of the actuator, measured in centimetres, is calculated for mutual inductance measurements between sensors 3, 4 and based on calibration function from Fig. 5.

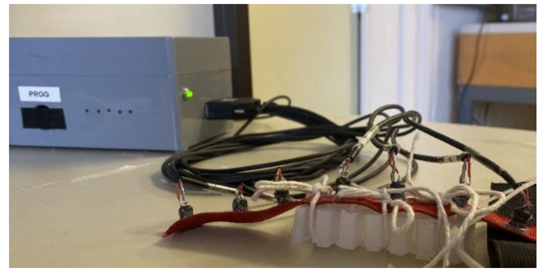

(a)

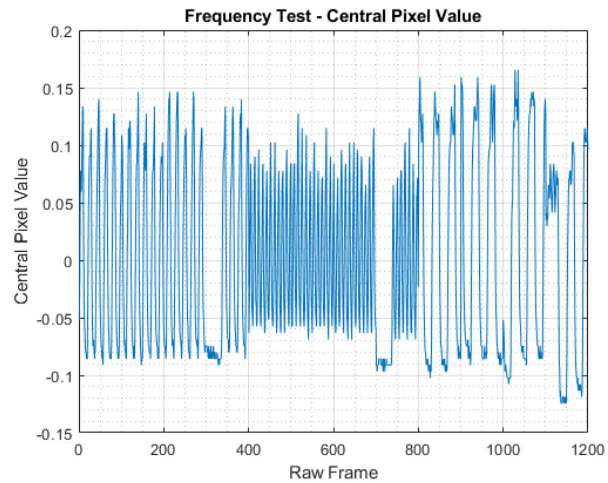

(b)

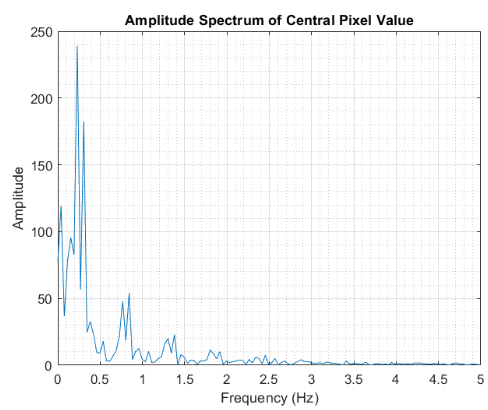

(c)

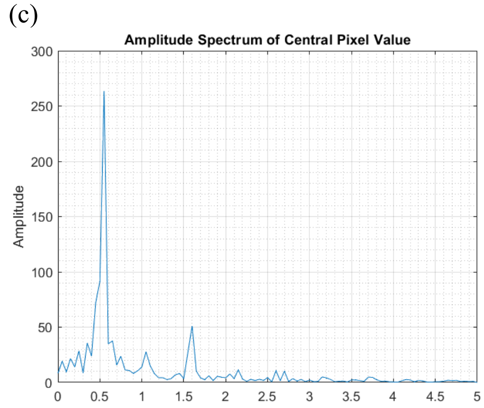

(d)

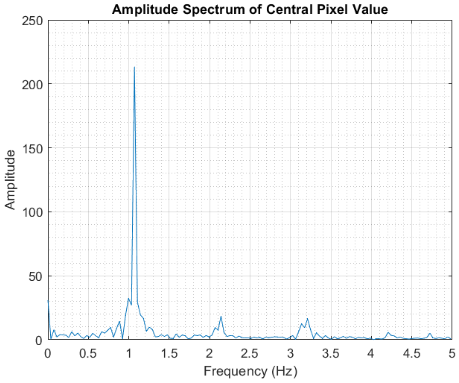

(e)

Fig. 14: The sensor position and shear force applied to a linear array with various frequencies (a) sensor and actuator setup, (b) displacement in the time domain, (c) frequency domain representation of entire displacement from part (b), (d) The slow segment from frame 800 to the end, and (e) the frequency domain response from 1-300 frames.

V. Discussions and Outlook

As the field of soft robots has progressed with more and more sophisticated actuation, there is a clear need for robust sensors to control those actions. Soft robotics uses deformable materials allowing shape changes and enabling conformable physical contact for manipulation. Yet, with the introduction of soft and stretchable materials to robotic systems comes a myriad of challenges for sensing strategies and their integration. This includes sensing based on various physical principles and often a combination of a wide variety of sensors. The sensors need to be able to capture stretching, be of high resolution, and also able to cover large area. This paper demonstrates the principle operation of a versatile shape-sensing tool based on mutual inductance data from an array of magnetic sensors. While the more in-depth modeling work will be the subject of future studies, the deployability and further miniaturization of the sensor system needs also be considered in follow-up studies. In that sense, the array can be fully embedded in the soft actuating materials. Clearly, the inductive array sensor with its inherent 3D shape-capturing capability will become a critical shape-sensing tool. While attempts are made to quantify and correlated various shape and function parameters there is room for further quantification and verification. In the future study when a case application of the sensor array is linked to a possible use case such a quantification can be further enhanced. Sensor array optimization may be needed for a given application, both computational modeling of the sensor array and SNR analysis from the measurement system cab e heo with such an optimization.

VI. Conclusions

The paper introduces a new shape-sensing array based on mutual inductance data. The fundamental operations were shown on a proof of concept for the proposed sensor system and related algorithms. Quantification of normal force applied to the 2D surface sensor tension and shear force is carried out by means of a calibration function. Several dynamical tests are done with varying force per frame demonstrating the real-time performance of inversion and calibration algorithms. With an actuated system we were able to show multiple frequencies of displacement from actuation modes from measured data. Several applications motivated this study, which will no doubt benefit from this novel sensing mechanism.

References

1. H. Griffiths, “Magnetic induction tomography”, Meas. Sci. Technol., Vol. 12: pages 1126–1131, Dec. 2001.

2. L. Ma, M. Soleimani, “Magnetic induction tomography methods, and applications: A review”, *Meas. Sci. Technol. 28*, 072001, 2007.

3. J. Avery, D. Shulakova, M. Runciman, G. P. Mylonas, and A. Darzi, “Tactile Sensor for Minimally Invasive Surgery Using Electrical Impedance Tomography”, IEEE Trans. Med. Robot. Bionics, vol. 2, no. 4, pp. 561–564, Nov. 2020

4. M. J. Kern, P. Sorajja, M. J. Lim, and M. J. Preceded by: Kern, “The interventional cardiac catheterization handbook”, Elsevier, 978-0-323-47671-3, 2017

5. L. Robertson, K. I. Paraskevas, and M. Stewart, “Angioplasty and stenting for a peripheral arterial disease of the lower limbs: An overview of Cochrane Reviews”, Cochrane Database Syst. Rev., vol. 2017, no. 2, 2017

6. D. Rus and M. T. Tolley, “Design, fabrication, and control of soft robots ”, Nature, vol. 521, pp. 467–475, May 2015.

7. C. Laschi, B. Mazzolai, and M. Cianchetti, “Soft robotics: Technologies and systems pushing the boundaries of robot abilities”, Sci. Robot., vol. 1, no. 1, Dec. 2016, Art. no. eaah3690,

8. D. Hu, H. Li, F. Giorgio-Serchi , and Y. Yang , “Coupling Field Simulation of Soft Capacitive Sensors Toward Soft Robot Perception”, IEEE Sensor Journal, Vol. 23, No. 10, 2023.

9. G. Ma, M. Soleimani, “A versatile 4D capacitive imaging array: a touchless skin and an obstacle-avoidance sensor for robotic applications ”, *Scientific Reports*, *10*(1), 1-9, 2020

10. W. Xin, F. Zhu , P. Wang , Z. Xie , Z. Tang , C. Laschi , “Electrical Impedance Tomographic Shape Sensing for Soft Robots”, IEEE Robotics and Automation Letters, Vol. 8, No. 3, 2023.

11. L. Wang, D. Jones, G. .J Chapman, H. J. Siddle, D. A. Russell, A. Alazmani, and P. Culmer, “An Inductive Force Sensor for In-Shoe Plantar Normal and Shear Load Measurement”, IEEE Sensors Journal, 20 (22). pp. 13318-13331, 2020

12. G. Dingley, M. Cox, M. Soleimani, “EM-skin: an artificial robotic skin using magnetic inductance tomography”, IEEE Transactions on Instrumentation and Measurement, *72*, 1, 2023.

13. B. Shih et al., “Electronic skins and machine learning for intelligent soft robots”, Sci. Robot., vol. 5, no. 41, 2020, Art. no. eaaz9239.

14. L. A. Garcia-Garcia, G. Valsamakis, P. Kreitmair, N. Munzenrieder, and D. Roggen, “Inferring complex textile shape from an integrated carbon black infused ecoflex-based bend and stretch sensor array”, in Proc. Adjunct ACM Int. Joint Conf. Pervasive Ubiquitous Comput. Proc. ACM Int. Symp. Wearable Comput., Virtual USA, pp. 298–303, 2021.

15. P. Mittendorfer and G. Cheng, “3D surface reconstruction for robotic body parts with artificial skins”, in Proc. IEEE/RSJ Int. Conf. Intell. Robots Syst., pp. 4505–4510, 2012.

16. S. I. Babic, F. Sirois, and C. Akyel, “Validity check of mutual induatce formulas for circular filamant with lateral and angaular mislaigmnets”, Progress In Electromagnetics Research M, Vol. 8, 15–26, 2009

17. F.W. Grover, “The Calculation of the Mutual Inductance of Circular Filaments in Any Desired Positions”, Proceedings of the I.R.E., 620–629, Oct. 1944

18. S. Butterworth, “On the coefficients of mutual induction of eccentric coils”, Philosophical Magazine, Series 6, Vol. 31, 443– 454, 1916.